

Ensemble Inequivalence in Long-Range Quantum Spin Systems

Daniel Arrufat-Vicente,^{1,*} David Mukamel,² Stefano Ruffo,^{3,4,5} and Nicolò Defenu¹

¹*Institute for Theoretical Physics, ETH Zürich, Wolfgang-Pauli-Str. 27, 8093 Zürich, Switzerland*

²*Department of Physics of Complex Systems, Weizmann Institute of Science, Rehovot 7610001, Israel*

³*Istituto dei Sistemi Complessi, Consiglio Nazionale delle Ricerche,*

Via Madonna del Piano 10, I-50019 Sesto Fiorentino, Italy

⁴*INFN, Sezione di Firenze*

⁵*SISSA, Via Bonomea 265, I-34136 Trieste, Italy*

(Dated: April 22, 2025)

Ensemble inequivalence occurs when a system's thermodynamic properties vary depending on the statistical ensemble used to describe it. This phenomenon is known to happen in systems with long-range interactions and has been observed in many classical systems. In this study, we provide a detailed analysis of a long-range quantum ferromagnet spin model that exhibits ensemble inequivalence. At zero temperature ($T = 0$), the microcanonical phase diagram matches that of the canonical ensemble. However, the two ensembles yield different phase diagrams at finite temperatures. This behavior contrasts with the conventional understanding in statistical mechanics of systems with short-range interactions, where thermodynamic properties are expected to align across different ensembles in the thermodynamic limit. We discuss the implications of these findings for synthetic quantum long-range platforms, such as atomic, molecular, and optical (AMO) systems.

I. INTRODUCTION.

The study of the equilibrium and dynamical behavior of long-range interacting quantum systems has recently attracted significant attention of the research community. This interest is partly driven by advances made in the control, manipulation, and observation of atomic, molecular, and optical (AMO) systems, where long-range interaction among microscopic constituents is a central feature [1–8]. Interactions are typically classified as long-range whenever the two-body interaction potential $V(r)$ between the microscopic constituents decays as a power law of the distance r , $V(r) \propto r^{-\alpha}$, with $\alpha > 0$ sufficiently small.

The behavior of such systems is deeply influenced by the exponent α . When $\alpha > \alpha_*$, where α_* is a universal threshold, the critical behavior of a system in equilibrium resembles that of short-range interacting system. Conversely, in d -dimensional systems with $d < \alpha < \alpha_*$, the scaling near phase transitions is altered by the long-range couplings [9–16]. Lastly, when $\alpha < d$, which is the strong long-range regime, standard thermodynamics breaks down. To recover the extensivity of energy, a rescaling factor, often referred to as Kac's rescaling, becomes necessary. This, however, does not ensure additivity of thermodynamic functions, resulting in unusual thermodynamic behavior.

In classical systems, this latter regime is characterized by hallmark phenomena such as *quasi-stationary states* (QSSs) [17–20] and *ensemble inequivalence* [21]. Quasi-stationary states are metastable states that slowly decay to the equilibrium state on timescales that diverge with system size. Ensemble inequivalence, on the other hand, refers to the fact that the thermodynamic behavior of the system becomes ensemble-dependent. This feature is the central focus of the present work. Ensemble inequivalence takes place whenever the microcanonical entropy becomes non concave with respect to the energy, so

that the canonical thermodynamic potential and the microcanonical entropy cannot be connected by a *Legendre transformation*. This implies regions with negative specific heat, which is a phenomenon known to be present during stellar formation [22].

In quantum systems, the statistical mechanics of strong long-range interactions remains to a large extent underexplored, with most of its progress inspired by the study of quasi-classical regimes. For instance, theoretical evidence of quantum QSSs has emerged [23–25]. Ergodicity breaking, another intriguing feature of long-range physics, is more pronounced in the microcanonical ensemble and has been observed in both classical and quantum contexts [26–29]. A comprehensive universal picture for these multifaceted theoretical evidences has just emerged [30–32].

Recently, a quantum spin model has been introduced and demonstrated to exhibit distinct canonical and microcanonical phase diagrams [33]. The model comprises quantum spins with fully connected long-range interactions and multi-spin coupling. It exhibits a paramagnetic to ferromagnetic phase transition which, depending on the interaction parameters, is either first order or continuous. The manifolds of the two transition types are separated by tricritical points. While the two ensembles yield identical $T = 0$ phase diagrams, their finite-temperature phase diagrams differ significantly. In Ref. [33] the critical and tricritical manifolds have been calculated, demonstrating that the two ensembles exhibit rather distinct tricritical manifolds. The first-order transition manifolds were only drawn schematically based on some general arguments.

Here, we present an alternative method for calculating the canonical free energy and the microcanonical entropy, yielding the full phase diagrams including the first order transitions. We also present numerical evidence that shows how negative specific heat emerges near the first order transition lines. The analysis is carried out by mapping the quantum problem onto a classical one with the caveat that one has to add an additional time direction. This is done by means of a Suzuki–Trotter decomposition that allows us to disentangle non-commuting terms

* darrufat@phys.ethz.ch

of the Hamiltonian. Such approach has already been used in many other setups and is believed to be exact for long-range interacting systems [34–36].

The significance of this study is underscored by the growing interest in controlling multi-body interactions in quantum many-body systems, particularly within the AMO community [37, 38]. Quantum tricritical points, naturally arising in such systems [39], are of special relevance. Experimental AMO platforms such as dipolar atom/molecule ensembles [40–42] and cold atoms in cavities [7] provide settings to explore ensemble inequivalence. Notably, cavity-mediated interactions create globally flat potentials, making them ideal for experimentally testing our predictions [25, 43, 44]. Recent cavity QED experiments, for example, have probed the pre-thermalization dynamics of long-range systems [45]. It is also important to point out that, fully connected quantum Hamiltonians hold promise for optimizing classical combinatorial problems via adiabatic quantum computing [46].

II. THE MODEL.

Our findings apply to a concrete example of long-range quantum system, where the extension of the classical picture to the quantum realm can be carried out explicitly. Following Ref. [33] we introduce the Hamiltonian of a long-range quantum ferromagnetic spin-1/2 chain with 4-spin interactions

$$\mathcal{H} = -\frac{J}{N} \left(\sum_{\ell} \sigma_{\ell}^z \right)^2 - h \sum_{\ell} \sigma_{\ell}^x - \frac{K}{N^3} \left(\sum_{\ell} \sigma_{\ell}^z \right)^4, \quad (1)$$

where the summations run over all sites of the lattice $\ell \in \{1, \dots, N\}$. The operators σ_{ℓ}^{μ} correspond to the $\mu = x, y, z$ Pauli matrices at site ℓ :

$$\sigma_{\ell}^x = \begin{pmatrix} 0 & 1 \\ 1 & 0 \end{pmatrix}, \quad \sigma_{\ell}^y = \begin{pmatrix} 0 & -i \\ i & 0 \end{pmatrix}, \quad \sigma_{\ell}^z = \begin{pmatrix} 1 & 0 \\ 0 & -1 \end{pmatrix}. \quad (2)$$

For the remainder of this discussion, we focus on the fully ferromagnetic case with $J, K > 0$. The sign of h plays no role since it can be compensated by an appropriate rotation.

We define the vector operator

$$\mathbf{S} = \frac{1}{2} \sum_{\ell} \boldsymbol{\sigma}_{\ell}, \quad (3)$$

where the boldface notation $\mathbf{S} = (S^x, S^y, S^z)$ and similarly $\boldsymbol{\sigma} = (\sigma^x, \sigma^y, \sigma^z)$ denotes vector representation. Using this operator, the Hamiltonian can be expressed as

$$\mathcal{H} = -\frac{4J}{N} (S^z)^2 - 2hS^x - \frac{16K}{N^3} (S^z)^4. \quad (4)$$

In the $K \rightarrow 0$ limit, the Hamiltonian in Eq.(1) simplifies to the well-known Lipkin-Meshkov-Glick (LMG) model [47–49]. At zero temperature ($T = 0$), this system features a quantum critical point at $h = h_c = 2J$, signaling a phase transition from a paramagnetic phase, where spins align along the x -axis, to a ferromagnetic phase with nonzero magnetization component along the z -axis. Note that while the Hamiltonian in Eq.(1) is extensive

due to the re-scaling of the interactions, it still remains non-additive and therefore can accommodate ensemble inequivalence.

Hamiltonians akin to Eq.(1) have been employed to investigate a variety of physical systems under both canonical and microcanonical ensembles. In the canonical framework, the quantum critical behavior of the Dicke model [50], which describes the interaction between the motional degrees of freedom of a Bose gas and the standing wave field of an optical cavity [51, 52], coincides with the one of our LMG model [53, 54]. Furthermore, spin models like Eq.(1) can be experimentally realized by coupling atomic internal states to the cavity field [55–58].

Alternatively, microcanonical ensemble representations of Eq.(1) describe systems such as coupled Bose-Einstein condensates (BECs) or Bose-Hubbard models in doublewell configurations [59], spin-1 BECs [60–64], and Rydberg atoms in the blockade regime [65–69]. Thus, examining the model in Eq.(1) under both canonical and microcanonical ensembles is of significant interest.

A distinctive aspect of the Hamiltonian in Eq.(1) is the incorporation of multi-spin interactions. While past research has primarily addressed the $K \rightarrow 0$ limit, investigating the general case aligns with current experimental attempts aimed at achieving quantum control of multi-body interactions [70, 71]. These interactions have already been used to model order-disorder transitions in ferroelectrics [72].

To explore the equilibrium properties of this system, we analyze it below within both the canonical and microcanonical ensembles, focusing on their respective thermodynamic potentials.

III. MODEL ANALYSIS.

In what follows, we compute the free-energy and entropy of the model, starting by computing the canonical partition function Z at temperature $k_B T = \beta^{-1}$ and the phase-space volume Ω with fixed energy E

$$Z(\beta, J, h, K) = \text{Tr} [e^{-\beta \mathcal{H}}], \quad (5)$$

$$\Omega(E, J, h, K) = \text{Tr} [\delta(E - \mathcal{H})]. \quad (6)$$

A. Canonical ensemble.

For the canonical partition function we get

$$\begin{aligned} Z &= \sum_{\{\vec{\tau}\}} \langle \vec{\tau} | \left(e^{-\beta H_z + \beta h \sum_i \sigma_i^x} \right) | \vec{\tau} \rangle \\ &= \lim_{N_s \rightarrow \infty} \text{Tr} \left[e^{-\frac{\beta}{N_s} H_z + \frac{\beta}{N_s} h \sum_i \sigma_i^x} \right]^{N_s}, \end{aligned} \quad (7)$$

where H_z is the part of the Hamiltonian (1) diagonal in the z basis, $H_z = -\frac{4J}{N} (S^z)^2 - \frac{16K}{N^3} (S^z)^4$, and $|\vec{\tau}\rangle$ represents a possible z -component Ising spin configuration, $\vec{\tau} \equiv |\uparrow, \uparrow, \downarrow, \dots\rangle$, which spans a complete orthogonal basis of the total Hilbert space. In the second line of this equation we have represented Z by a product of N_s Trotter slices. Introducing a closure relation in between each Trotter slice, $\mathbf{1} = \sum_{\{\vec{\tau}\}} |\vec{\tau}\rangle \langle \vec{\tau}|$ and noting that in the limit

$N_s \rightarrow \infty$ one can split the exponential, we get,

$$\begin{aligned} Z &= \sum_{\{\vec{\tau}(\alpha)\}} \prod_{\alpha=1}^{N_s} \langle \vec{\tau}(\alpha) | e^{-\frac{\beta}{N_s} H_z(\alpha)} e^{\frac{\beta}{N_s} \sum_i h \sigma_i^x(\alpha)} | \vec{\tau}(\alpha+1) \rangle \quad (8) \\ &= \sum_{\{\vec{\tau}(\alpha)\}} \prod_{\alpha=1}^{N_s} e^{-\frac{\beta}{N_s} E_z(\alpha)} \prod_{\alpha=1}^{N_s} \langle \vec{\tau}(\alpha) | e^{\frac{\beta}{N_s} \sum_i h \sigma_i^x(\alpha)} | \vec{\tau}(\alpha+1) \rangle. \end{aligned}$$

The index α in $|\vec{\tau}(\alpha)\rangle$ labels the Trotter step. The trace in Eqs. (5) and (6), imposes periodic boundary conditions on the additional “time” direction, $\vec{\tau}(N_s+1) = \vec{\tau}(1)$, where we also used $H_z |\vec{\tau}(\alpha)\rangle = E_z(\alpha) |\vec{\tau}(\alpha)\rangle$.

We proceed by defining the magnetization order parameter for each of the α slices,

$$m_z(\alpha) = \frac{1}{N} \sum_i \sigma_i^z(\alpha), \quad (9)$$

and introducing N_s copies of the delta function $N \int dm_z \delta(Nm_z - \sum_i \sigma_i^z) f(Nm_z) = f(\sum_i \sigma_i^z)$. We then make use of the Fourier representation of the delta function

$$\delta(x) = \frac{1}{2\pi i} \int_{-i\infty}^{+i\infty} e^{\lambda x} d\lambda. \quad (10)$$

The partition sum is then given by

$$\begin{aligned} Z &= \lim_{N_s \rightarrow \infty} \int \prod_{\alpha=1}^{N_s} \frac{dm_z(\alpha) d\lambda(\alpha)}{2\pi i N_s / (\beta N)} e^{-\frac{\beta N}{N_s} \sum_{\alpha=1}^{N_s} (e(m_z(\alpha)) + \lambda(\alpha) m_z(\alpha))} \times \sum_{\vec{\tau}(1), \dots, \vec{\tau}(N_s)} \prod_{\alpha=1}^{N_s} \langle \vec{\tau}(\alpha) | e^{\frac{\beta}{N_s} \sum_{i=1}^N [\lambda(\alpha) \sigma_i^z + h \sigma_i^x]} | \vec{\tau}(\alpha+1) \rangle \\ &= \lim_{N_s \rightarrow \infty} \int \prod_{\alpha=1}^{N_s} \frac{dm_z(\alpha) d\lambda(\alpha)}{2\pi i N_s / (\beta N)} \exp \left[-N \left(\frac{\beta}{N_s} \sum_{\alpha=1}^{N_s} (e(m_z(\alpha)) + \lambda(\alpha) m_z(\alpha)) - \ln \text{Tr} \prod_{\alpha=1}^{N_s} e^{\frac{\beta}{N_s} (\lambda(\alpha) \sigma_i^z + h \sigma_i^x)} \right) \right], \quad (11) \end{aligned}$$

where we have defined $e(m_z) \equiv E_z/N = -Jm_z^2 - Km_z^4$. At this point, we focus on thermal equilibrium and we assume that the dominant contribution to the integral derives from values of $m_z(\alpha)$ and $\lambda(\alpha)$ independent of α , to obtain

$$Z \propto \int dm_z d\lambda \exp \left[N\beta \left(Jm_z^2 + Km_z^4 - \lambda m_z + \frac{1}{\beta} \ln 2 \cosh \left(\sqrt{\lambda^2 + h^2} \right) \right) \right], \quad (12)$$

Eq. (12) (and the corresponding equation (20) for the microcanonical ensemble) can be computed by a saddle point approximation which becomes exact in the thermodynamic limit due to the factor of N on the exponential. The free energy reduces to,

$$\begin{aligned} f(\beta, J, h, K) &= -Jm_z^2 - Km_z^4 + \lambda m_z \\ &\quad - \frac{1}{\beta} \ln \left(2 \cosh \left(\beta \sqrt{h^2 + \lambda^2} \right) \right). \quad (13) \end{aligned}$$

In order to apply the saddle point method we deform the contour of integration of λ from $(-i\infty, +i\infty)$ to $(-i\infty+a, +i\infty+a)$, where a is a real number, chosen such that the new contour passes through the saddle point of the free energy f . The saddle point condition imposes the free-energy to be an extremum with respect to the variational parameters m_z and λ

$$\frac{\partial f}{\partial \lambda} = 0: \quad m_z = \frac{\lambda}{\sqrt{\lambda^2 + h^2}} \tanh \left(\beta \sqrt{\lambda^2 + h^2} \right), \quad (14)$$

$$\frac{\partial f}{\partial m_z} = 0: \quad \lambda = 2Jm_z + 4Km_z^3. \quad (15)$$

For later convenience we write the free-energy in terms of a single order parameter m_z

$$\begin{aligned} f(\beta, J, h, K) &= Jm_z^2 + 3Km_z^4 \\ &\quad - \frac{1}{\beta} \ln \left(2 \cosh \left(\beta \sqrt{h^2 + (2Jm_z + 4Km_z^3)^2} \right) \right). \quad (16) \end{aligned}$$

In Section IV we analyze this free energy to obtain the canonical phase diagram.

B. Microcanonical ensemble.

For the microcanonical ensemble we first need to introduce a Fourier representation of the Dirac delta, as it was done in the preceding section,

$$\Omega = \int_{-i\infty+a}^{+i\infty+a} \frac{d\gamma}{2\pi i} \sum_{\{\vec{\tau}\}} \langle \vec{\tau} | \left(e^{\gamma(E - H_z + h \sum_i \sigma_i^x)} \right) | \vec{\tau} \rangle. \quad (17)$$

By following the same procedure described for the canonical ensemble, we can rewrite the phase-space volume Ω as,

$$\begin{aligned} \Omega &= \int \frac{d\gamma}{2\pi i} \sum_{\{\vec{\sigma}(\alpha)\}} \prod_{\alpha=1}^{N_s} e^{\gamma(E - E_z(\alpha))/N_s} \\ &\quad \times \prod_{\alpha=1}^{N_s} \langle \vec{\tau}(\alpha) | e^{\frac{\gamma h}{N_s} \sum_i \sigma_i^x(\alpha)} | \vec{\tau}(\alpha+1) \rangle. \quad (18) \end{aligned}$$

It is important to note that, while in the canonical expression β is a fixed parameter, here, the corresponding parameter, γ , is being integrated over the entire range $[-\infty, \infty]$. Therefore, even though it was handy to introduce Dirac representations scaled with a β factor in the canonical derivation, we cannot naively proceed in the same manner for the computation of Ω . Taking this fact into account, we instead introduce unscaled Dirac

representations as

$$\Omega = \lim_{N_s \rightarrow \infty} \int \frac{d\gamma}{2\pi i} \int \prod_{\alpha=1}^{N_s} \frac{dm_z(\alpha) d\lambda(\alpha)}{2\pi N_s} \exp \left[N \left(\frac{1}{N_s} \sum_{\alpha=1}^{N_s} (\gamma(\varepsilon - e(m_z(\alpha))) - \lambda(\alpha)m_z(\alpha)) + \ln \text{Tr} \prod_{\alpha=1}^{N_s} e^{\frac{1}{N_s}(\lambda(\alpha)\sigma_i^z + \gamma h \sigma_i^x)} \right) \right], \quad (19)$$

In the same spirit as before we assume that the dominant contribution comes from values of $m_z(\alpha)$ and $\lambda(\alpha)$ independent of α

$$\Omega \propto \int d\gamma dm_z d\lambda \exp \left[N \left(\gamma (Jm_z^2 + Km_z^4 + \varepsilon) - \lambda m_z + \ln 2 \cosh \left(\sqrt{\lambda^2 + \gamma^2 h^2} \right) \right) \right]. \quad (20)$$

In the microcanonical situation we observe that we have an additional order parameter γ , which, as we know, has to account for the fact that in the microcanonical ensemble the energy is fixed. Again, due to the factor of N in the exponential, the entropy $\mathcal{S} \equiv 1/N \ln \Omega$ is completely dominated by values of γ, λ, m_z that maximize the entropy.

$$\mathcal{S}(\varepsilon, J, h, K) = \gamma (Jm_z^2 + Km_z^4 + \varepsilon) - \lambda m_z + \ln 2 \cosh \left(\sqrt{\lambda^2 + \gamma^2 h^2} \right), \quad (21)$$

with

$$\partial_\lambda \mathcal{S} = 0 : m_z = \frac{\lambda \tanh \left(\sqrt{\lambda^2 + \gamma^2 h^2} \right)}{\sqrt{\lambda^2 + \gamma^2 h^2}}, \quad (22)$$

$$\partial_{m_z} \mathcal{S} = 0 : \frac{\lambda}{\gamma} = 2Jm_z + 4Km_z^3, \quad (23)$$

$$\partial_\gamma \mathcal{S} = 0 : \varepsilon = -Jm_z^2 - Km_z^4 - \frac{\gamma h^2}{\sqrt{\lambda^2 + \gamma^2 h^2}} \tanh \left(\sqrt{\lambda^2 + \gamma^2 h^2} \right). \quad (24)$$

Substituting these relations into Eq.(21), and following the steps outlined at the beginning of Appendix A, one can rewrite the entropy as a function of the magnetization m_z and energy ε

$$\mathcal{S}(J, h, K) = -\text{arctanh} \left(\sqrt{m_z^2 + \frac{(\varepsilon + Jm_z^2 + Km_z^4)^2}{h^2}} \right) \times \sqrt{m_z^2 + \frac{(\varepsilon + Jm_z^2 + Km_z^4)^2}{h^2}} + \ln \left(\frac{2h}{\sqrt{h^2 - m_z^2 h^2 - (\varepsilon + Jm_z^2 + Km_z^4)^2}} \right). \quad (25)$$

IV. THE PHASE DIAGRAM.

In the following we analyze the finite-temperature phase diagrams in both ensembles.

A. Canonical ensemble.

Let us begin by determining the location of the second-order phase transition line and the tricritical point. We start by expanding Eq. (16) in terms of m_z^2

$$f(\beta, J, h, K) \approx f_0 + b_2 m_z^2 + b_4 m_z^4 + \mathcal{O}(m_z^6), \quad (26)$$

where

$$b_2 = J - 2J^2 \frac{\tanh(\beta h)}{h}, \quad (27)$$

$$b_4 = 3K - \frac{2J}{h^3} \left(\beta h J^3 \cosh^{-2}(\beta h) + (4h^2 K - J^3) \tanh(\beta h) \right), \quad (28)$$

setting $b_2 = 0$ yields the second order transition and, consequently, setting both $b_2 = b_4 = 0$ determines the tricritical point,

$$\frac{h_c}{2J} = \tanh(\beta h_c), \quad (29)$$

$$K_{tcp} = \frac{J^3}{h_c^2} + \frac{\beta J^2}{2} \left(1 - \frac{4J^2}{h_c^2} \right). \quad (30)$$

Expanding near low temperatures we obtain

$$b_2 = 0 : h_c[CE] = 2J(1 - 2e^{-4\beta J}), \quad (31)$$

$$b_4 = 0 : K_{tcp}[CE] = \frac{J}{4} - 2\beta J^2 e^{-4\beta J}. \quad (32)$$

which coincides with the result reported in [33]. It is worthwhile noting that the critical field h/J does not depend on K/J , but rather is only a function of the temperature.

The first order transition line is determined by finding numerically for which values of $(K/J, h/J)$ the system undergoes a discontinuous change to a state with non-vanishing magnetization m_z^* . This happens when $f(m_z = 0)$ and $f(m_z = m_z^*)$ are both global minima of the free energy, i.e.

$$f(m_z = 0) = f(m_z^*), \quad \partial_{m_z} f(m_z)|_{m_z=0} = \partial_{m_z} f(m_z)|_{m_z=m_z^*} = 0, \quad (33)$$

yielding the following conditions

$$m_z^* = \frac{\tanh \left(\beta \sqrt{h^2 + (2Jm_z^* + 4Km_z^{*3})^2} \right)}{\sqrt{h^2 + (2Jm_z^* + 4Km_z^{*3})^2}} (2Jm_z^* + 4Km_z^{*3}),$$

$$Jm_z^{*2} + 3Km_z^{*4} + \frac{1}{\beta} \ln(\cosh \beta h) = \frac{1}{\beta} \ln \left(\cosh \left(\beta \sqrt{h^2 + (2Jm_z^* + 4Km_z^{*3})^2} \right) \right), \quad (34)$$

whose solution is found numerically and reported in Fig. 1.

B. Microcanonical ensemble.

To determine the second-order phase transition line and the tricritical point in the microcanonical ensemble we expand Eq. (25) in terms of m_z^2 and again locate for which conditions the coefficients of the expansion vanish.

$$\mathcal{S}(\varepsilon, J, h, K) \approx s_0 + a_2 m_z^2 + a_4 m_z^4 + \mathcal{O}(m^6), \quad (35)$$

with

$$a_2 = -\frac{(h^2 + 2\varepsilon J)\text{arctanh}(\varepsilon/h)}{2h\varepsilon}, \quad (36)$$

$$a_4 = \frac{h^2 + 2\varepsilon J}{8\varepsilon^2(\varepsilon^2 - h^2)} \quad (37)$$

$$-\frac{h^4 + 4\varepsilon h^2 J - 8\varepsilon^3 K}{8h\varepsilon^3} \text{arctanh}(\varepsilon/h),$$

The resulting critical line is found by imposing

$$h^2 + 2\varepsilon J = 0, \quad (38)$$

which, together with

$$h^4 + 4\varepsilon h^2 J - 8\varepsilon^3 K = 0, \quad (39)$$

yields the tricritical point. In order to proceed and compare with the canonical ensemble, one has to express ε in terms of the temperature. Along the critical line, $m_z = 0$, the temperature is in direct connection with the energy,

$$\beta = \frac{\partial \mathcal{S}}{\partial \varepsilon} = -\frac{\text{arctanh}(\varepsilon/h)}{h}, \quad (40)$$

which gives

$$\varepsilon = -h \tanh \beta h. \quad (41)$$

Inserting expression (41) in (38), the microcanonical ([MCE]) critical line can be found by numerically solving

$$h_c[MCE] = 2J \tanh(\beta h_c). \quad (42)$$

Along the critical line, Eq. (39) yields the tricritical point at

$$K_{tcp}[MCE] = \frac{J}{4 \tanh(\beta h_c)^2}. \quad (43)$$

This expression, together with the respective result in the canonical ensemble, demonstrates the inequivalence of the two ensembles. While both ensembles yield the same expression for the critical lines, Eq.(29) and Eq(42), their tricritical points differ. At a fixed temperature, the canonical tricritical point, given by Eq. (32), occurs at a lower value of K/J than the corresponding microcanonical tricritical point, as shown in Fig.1, which presents the $(h/J, K/J)$ phase diagram at $\beta J = 2/3$. To determine the first-order transition lines we have to maximize the entropy with respect to the order parameter m_z at fixed energy. To compare with the canonical solution, one needs to fix the temperature instead of the energy. In order to do so we have to relate the energy to the temperature. However, for systems that present regions with negative specific heat, there is no one to one correspondence between energy and temperature. In this case, we

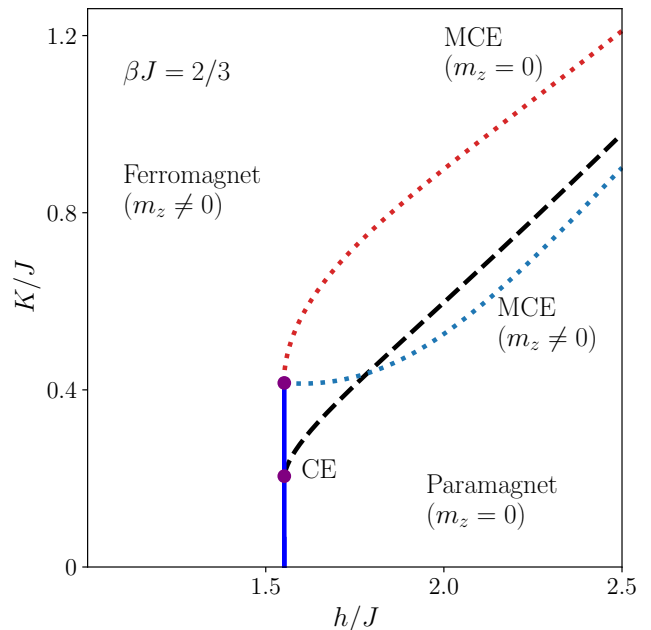


Figure 1: The canonical and microcanonical $(h/J, K/J)$ phase diagrams at a given temperature ($\beta J = 2/3$) are illustrated. The microcanonical critical line (solid blue) coincides with the canonical one but extends beyond the canonical tricritical point. The two microcanonical first order transition lines correspond, respectively, to either the $m_z = 0$ solution (dotted red), or to the spontaneously magnetized state $m_z = m_z^*$ (dotted blue). The canonical first order transition is depicted by the black dashed line.

can determine the temperature either by looking at the solution in the paramagnetic regime ($m_z = 0$) or at the solution in the ferromagnetic regime ($m_z = m_z^* \neq 0$), given, respectively, by

$$\beta = -\frac{\text{arctanh}(\varepsilon/h)}{h}, \quad (44)$$

$$\beta = -\frac{(\varepsilon + Jm_z^{*2} + Km_z^{*4})}{h\sqrt{h^2 m_z^{*2} + (\varepsilon + Jm_z^{*2} + Km_z^{*4})^2}} \quad (45)$$

$$\times \text{arctanh} \left(\sqrt{m_z^{*2} + \frac{(\varepsilon + Jm_z^{*2} + Km_z^{*4})^2}{h^2}} \right).$$

Similarly to the canonical ensemble, in order to determine the first order transition line, we demand the entropy \mathcal{S} to have three global maxima at $m_z = 0, \pm m_z^*$, i.e.

$$\begin{aligned} h^2 + (\varepsilon + Jm_z^{*2} + Km_z^{*4})(2J + 4Km_z^{*2}) &= 0, \\ h^2 m_z^{*2} + (\varepsilon + Jm_z^{*2} + Km_z^{*4})^2 &= \varepsilon^2. \end{aligned} \quad (46)$$

The first equation expresses the requirement that the solution $m_z = \pm m_z^*$ is a local extremum of the entropy, while the second equation results from the requirement that the entropies at $m_z = 0$ and $\pm m_z^*$ are equal. For given (J, h, K) these two equations are solved for ε and m_z^* , yielding the energy and the magnetization in the ordered state. Using these values in Eq. (44) and Eq. (45) to determine the two temperatures of the coexisting states, gives rise to the two first order transition lines reported

in Fig. 1. In combination with the canonical transition line, these two microcanonical lines complete the phase diagram schematically reported in [33].

In Fig. 2 we display the tricritical coupling K/J for both ensembles, (32) and (43), as a function of T/J . At $T = 0$, the tricritical points of the two ensembles coincide, but as the temperature increases, the canonical tricritical point varies more gradually. It is important to note that, while the magnetic field h/J varies along the two lines, its value at any given temperature is the same on both lines.

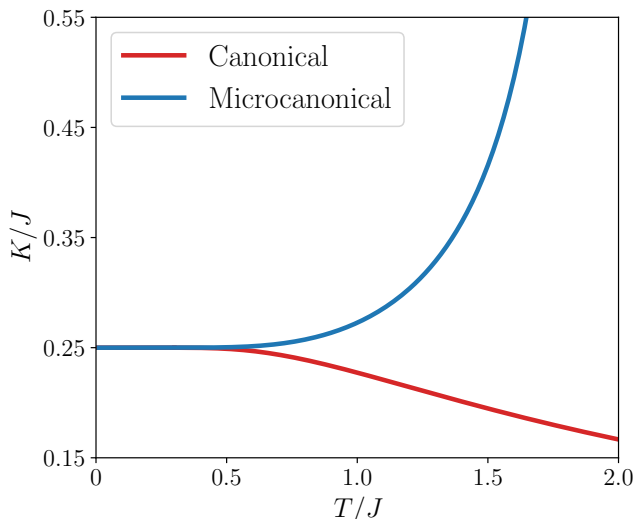


Figure 2: Tricritical point K/J against T/J in the canonical and microcanonical ensembles. Note that the field h/J varies along the lines, see Eqs. (29) and (42).

V. CALORIC CURVES

To complete and complement the study of the phase diagram in the microcanonical ensemble, we display in Fig. 3 the $(T/J, K/J)$ phase diagram for a given field h/J and the temperature-energy relation $T(\epsilon)$, in Fig. 4. As in Fig. 1, we see in Fig. 3 the two distinct tricritical points of the canonical and microcanonical ensembles

In Fig. 4 we display the caloric curves for $h/J \approx 1.55$ and several values of K/J . Noting that the critical temperature in both ensembles is independent of K/J and depends only on h/J . The value of h/J is arbitrarily chosen such that the temperature on the critical line and tricritical point in both ensembles is $\beta J = 2/3$. Each caloric curve is composed of two branches, a low-energy branch corresponding to the spontaneously magnetized state m_z^* and a high-energy one for the paramagnetic phase $m_z = 0$.

The two branches intersect where their respective entropies become equal. For $K/J \approx 0.19$, corresponding to the canonical tricritical point at $\beta J = 2/3$ (see Eqs. (29) and (30)), the lower energy branch has zero curvature at the intersection point (Fig. 4a). At this point, the specific heat of the magnetized phase diverges. For $K/J = 0.35$, where the system lies in between the canonical and the microcanonical tricritical points, an energy domain with

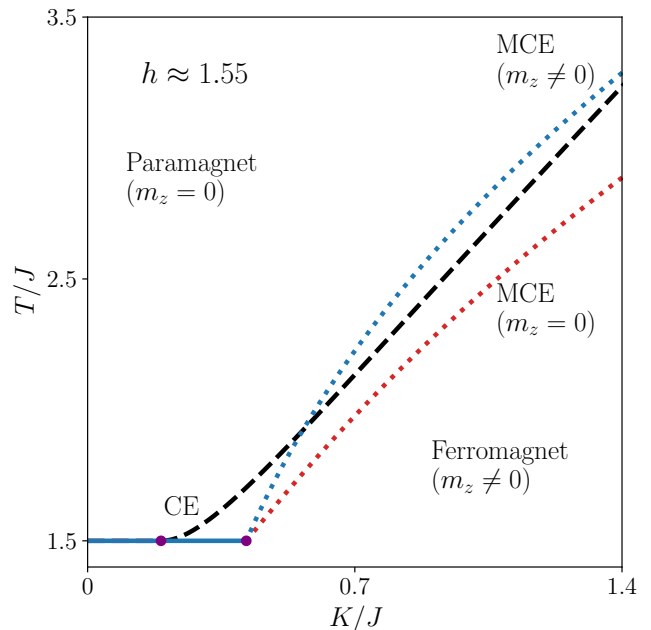


Figure 3: The canonical and microcanonical $(T/J, K/J)$ phase diagrams at a given $h/J \approx 1.55$ chosen such that the critical line and the two tricritical points take place at $\beta J = 2/3$. As in Fig. 1, the two microcanonical first order lines correspond, respectively, to either the $m_z = 0$ solution or to the spontaneously magnetized $m_z = m_z^*$ one.

negative specific heat in the microcanonical ensemble first arises with $\partial T/\partial \epsilon < 0$ (see Fig. 4b). Increasing K/J to $K/J \approx 0.41$ (Fig. 4c) the microcanonical tricritical point is reached, see Eqs. (42) and (43). Here, the slope of the lower energy branch of the caloric curve diverges at the tricritical point. At higher values of K/J a discontinuity develops (see Fig. 4d for $K/J = 1.40$) signaling a temperature jump at the transition.

VI. CONCLUSIONS

In this paper, we extend a previous study of the phase diagram of a model with long-range and multi-spin interactions. This model exhibits a paramagnetic to ferromagnetic quantum phase transition, featuring both first-order and second-order branches separated by tricritical points.

At $T = 0$, the phase diagram is solely determined by the ground state properties, resulting in identical phase diagrams for both ensembles. However, at finite temperatures, the phase diagrams separates. Specifically, we found that the tricritical point shifts upwards in the microcanonical description and downwards in the canonical description as the temperature increases. We also investigate the relationship between temperature T and energy ϵ in the microcanonical case, demonstrating that, for certain parameters, the model exhibits negative specific heat and temperature jumps near the first-order phase transition.

To understand the robustness of this effect, it would be valuable to explore the validity of these results in other quantum models, such as spin systems with long-range

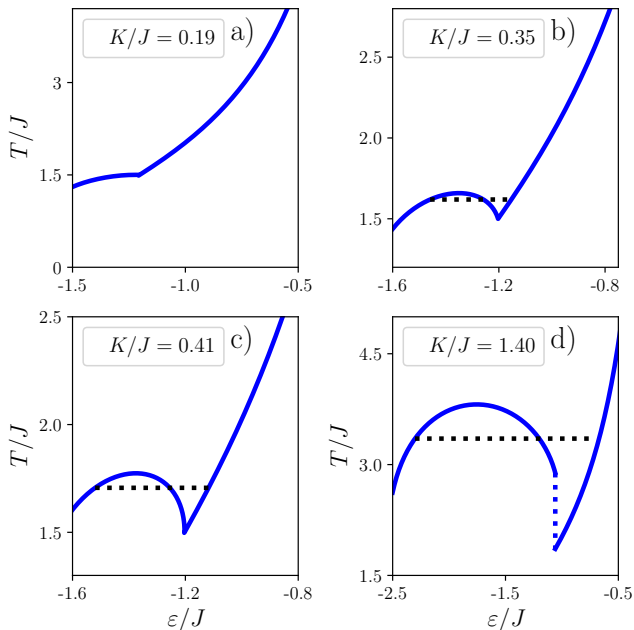


Figure 4: Temperature versus energy relation in the microcanonical ensemble for $h/J \approx 1.55$ and several values of K/J (see text). The horizontal line in panels (b-d) is the Maxwell construction in the canonical ensemble, which identifies the canonical first order transition temperature.

interactions where the interaction strength decays as a power-law with the distance.

As the field of AMO continues to advance, we anticipate that these results could be experimentally tested on quantum platforms, particularly in the context of cold atoms with cavity-mediated interactions. Specifically, the Hamiltonian in Eq. (1) for $K = 0$ is the paradigmatic Dicke model, which has already been used to describe certain cavity QED platforms [43, 73, 74]. Realizing the four-body interaction term at $K > 0$ may be achieved by leveraging recent findings on cavity-mediated pair creation [75].

ACKNOWLEDGMENTS

This research was supported in part by grant NSF PHY-1748958 to the Kavli Institute for Theoretical Physics (KITP). This research was funded by the Swiss National Science Foundation (SNSF) grant number 200021 207537, by the Deutsche Forschungsgemeinschaft (DFG, German Research Foundation) under Germany's Excellence Strategy EXC2181/1-390900948 (the Heidelberg STRUCTURES Excellence Cluster), the Swiss State Secretariat for Education, Research and Innovation (SERI), and by the Center for Scientific Excellence at the Weizmann Institute of Science. SR acknowledges support from the MUR PRIN2022 project BECQuMB Grant No. 20222BHC9Z.

Appendix A: Equivalence between methods.

In a previous study [33] a different approach was applied to calculate the free energy and the entropy of the model. To compute the thermodynamic potentials, they decompose the Hilbert space into different total spin sectors.

$$Z(\beta, J, h, K) = \sum_S g(S) \sum_{S^z=-S}^S \langle S, S^z | e^{-\beta \mathcal{H}} | S, S^z \rangle, \quad (\text{A1})$$

$$\Omega(E, J, h, K) = \sum_S g(S) \sum_{S^z=-S}^S \langle S, S^z | \delta(E - \mathcal{H}) | S, S^z \rangle. \quad (\text{A2})$$

Here S labels the total quantum spin (composed of N tensor products of $1/2$ -spins) and S_z the magnetization along the z direction. The factor $g(S)$ accounts for the degeneracy that comes from the multiple ways to arrange the microscopic $1/2$ -spins in order to form a total spin S [72]. For large spin S sectors, we can approximate the quantum partition function by a classical integral over the surface of a sphere with radius $S = M$ and parametrized such that $\mathbf{S} = M \mathbf{m}$, where $\mathbf{m} \equiv (m_x, m_y, m_z) = (\sin \theta \cos \phi, \sin \theta \sin \phi, \cos \theta)$ [76]. Moreover, in the thermodynamic limit, one can approximate the sum over S in Eq. (A1) and Eq. (A2) by an integral over the continuous variable of total spin s . Altogether and because of the mean-field nature of the problem, everything is dominated by a saddle point which enforces $\phi = 0$ and depends only on two variational parameters s and m_z

$$f(\beta, J, h, K) = \varepsilon - \mathcal{S}/\beta = -Js^2 m_z^2 - Ks^4 m_z^4 - hs \sqrt{1 - m_z^2} + \frac{1}{\beta} \left[\frac{1+s}{2} \ln \frac{1+s}{2} + \frac{1-s}{2} \ln \frac{1-s}{2} \right], \quad (\text{A3})$$

and

$$\mathcal{S} = -\frac{1+s}{2} \ln \left(\frac{1+s}{2} \right) - \frac{1-s}{2} \ln \left(\frac{1-s}{2} \right). \quad (\text{A4})$$

Note that the entropy in (A4) exactly corresponds to the logarithm of $g(S)$ for large N .

In what follows, we will show how, even though a priori very different, Eq. (A3) and Eq. (A4) give rise to the same phase diagrams as Eq. (16) and Eq. (25). We start by guiding the reader through the steps taken to derive Eq. (25) from (21). In order to find an expression for γ let us recall Eq. (24) for the energy

$$\varepsilon = -Jm_z^2 - Km_z^4 - \frac{h^2}{\sqrt{(\lambda/\gamma)^2 + h^2}} \tanh \left(\gamma \sqrt{(\lambda/\gamma)^2 + h^2} \right), \quad (\text{A5})$$

and the relation in Eq. (23)

$$\frac{\lambda}{\gamma} = 2Jm_z + 4Km_z^3. \quad (\text{A6})$$

We can then substitute the $(Jm_z^2 + Km_z^4 + \varepsilon)$ and m_z terms in the entropy reported in Eq. (21) to obtain

$$\mathcal{S}(\varepsilon, J, h, K) = -\sqrt{\lambda^2 + \gamma^2 h^2} \tanh \sqrt{\lambda^2 + \gamma^2 h^2} + \ln \left(2 \cosh \left(\sqrt{\lambda^2 + \gamma^2 h^2} \right) \right). \quad (\text{A7})$$

Moreover, by inverting the tangent in Eq. (A5) and substituting the λ/γ with Eq. (A6) we find

$$\gamma = -\operatorname{arctanh}\left(\frac{\varepsilon + Jm_z^2 + Km_z^4}{h^2}\sqrt{h^2 + (2Jm_z + 4Km_z^3)^2}\right) \times \frac{1}{\sqrt{h^2 + (2Jm_z + 4Km_z^3)^2}}. \quad (\text{A8})$$

Let us also note that by rewriting Eq. (24) as

$$\varepsilon + Jm_z^2 + Km_z^4 = -\frac{\gamma}{\lambda}\frac{h^2}{\sqrt{1 + h^2(\gamma/\lambda)^2}}\tanh\left(\sqrt{\lambda^2 + \gamma^2 h^2}\right), \quad (\text{A9})$$

and making use of Eq. (22) and Eq. (23), we can relate m_z and ε as follows

$$h^2 = -(2J + 4Km_z^2)(\varepsilon + Jm_z^2 + Km_z^4). \quad (\text{A10})$$

This equation, and the fact that $J, K \geq 0$, imply that $\varepsilon + Jm_z^2 + Km_z^4 \leq 0$. It allows us to rewrite the expression for γ in Eq.(A8) as

$$\gamma = \operatorname{arctanh}\left(\sqrt{m_z^2 + \frac{(\varepsilon + Jm_z^2 + Km_z^4)^2}{h^2}}\right) \times \frac{1}{\sqrt{h^2 + (2Jm_z + 4Km_z^3)^2}}. \quad (\text{A11})$$

Equivalently, making use of (23), this equation may be expressed as

$$\tanh\left(\sqrt{\lambda^2 + \gamma^2 h^2}\right) = \sqrt{m_z^2 + \frac{(\varepsilon + Jm_z^2 + Km_z^4)^2}{h^2}}, \quad (\text{A12})$$

which, in combination with the expression for the entropy given in Eq. (A7) and using the trigonometric relation

$$\cosh(\operatorname{arctanh}(x)) = \frac{1}{\sqrt{1-x^2}}, \quad (\text{A13})$$

leads to the expression given in Eq.(25) for the entropy.

In order to prove the equivalence between the two approaches of analyzing the model, let us notice that, minimizing the free-energy (Eq. (A3)) with respect to the parameters m_z and s , gives the following constraints,

$$2Js + 4Ks^3m_z^2 = \frac{h}{\sqrt{1-m_z^2}}, \quad (\text{A14})$$

$$\frac{1}{\beta}\operatorname{arctanh}(s) = 2Jsm_z^2 + 4Ks^3m_z^4 + h\sqrt{1-m_z^2}. \quad (\text{A15})$$

Plugging them back into Eq. (A3) allows us to rewrite the free-energy

$$f(\beta, J, h, K) = Js^2m_z^2 + 3Ks^4m_z^4 - \frac{s}{\beta}\operatorname{arctanh}(s) + \frac{1}{\beta}\left[\frac{1+s}{2}\ln\frac{1+s}{2} + \frac{1-s}{2}\ln\frac{1-s}{2}\right]. \quad (\text{A16})$$

Next, we make use of the following identity

$$\frac{1+s}{2}\ln\frac{1+s}{2} + \frac{1-s}{2}\ln\frac{1-s}{2} = \ln\frac{\sqrt{1-s^2}}{2} + \operatorname{stanh}^{-1}(s), \quad (\text{A17})$$

and Eq. (A15) is finally rewritten as

$$f(\beta, J, h, K) = Js^2m_z^2 + 3Ks^4m_z^4 - \frac{1}{\beta}\ln\left(2\cosh\left(\beta\sqrt{h^2 + (2Jsm_z + 4Ks^3m_z^3)^2}\right)\right), \quad (\text{A18})$$

where we have used the fact that $1 - \tanh(s)^2 = \operatorname{sech}(s)^2$ and combined Eq.(A14) and Eq.(A15) to notice that

$$s = \tanh\left(\beta\sqrt{h^2 + (2Jsm_z + 4Ks^3m_z^3)^2}\right).$$

This proves the equivalence between the results when rescaling the magnetization $m_z \equiv sm_z$. The equivalence can also be shown for the microcanonical ensemble by looking back at Eq. (22) and identifying

$$s = \tanh\left(\sqrt{\lambda^2 + \gamma^2 h^2}\right), \quad (\text{A19})$$

$$m_z = \frac{\lambda}{\sqrt{\lambda^2 + \gamma^2 h^2}}.$$

Rewriting Eq. (25) in terms of γ and λ

$$\mathcal{S}(J, h, K) = -\sqrt{\lambda^2 + \gamma^2 h^2}\tanh^{-1}\left(\sqrt{\lambda^2 + \gamma^2 h^2}\right) + \ln\frac{1}{\sqrt{1 - (\lambda^2 + \gamma^2 h^2)}}. \quad (\text{A20})$$

Looking back at Eq. (A17) and Eq.(A19), it is straightforward to see the equivalence with Eq. (A20) and Eq. (A4).

Appendix B: Maximization of the entropy.

In this section we show, in a straightforward way, how the maximization of the entropy that lead to Eq. (46) is obtained. We begin by pointing out how the entropy in Eq. (25) depends only on a single argument

$$\mathcal{S}(J, h, K) = -\sqrt{x}\operatorname{arctanh}(\sqrt{x}) + \ln\left(\frac{2}{\sqrt{1-x}}\right), \quad (\text{B1})$$

where

$$x \equiv m_z^2 + \frac{(\varepsilon + Jm_z^2 + Km_z^4)^2}{h^2}. \quad (\text{B2})$$

The entropy in Eq. (B1) is monotonically decreasing in the interval $x \in [0, 1]$ where the entropy is defined. Therefore, obtaining the maximum with respect to m_z is equivalent to

$$\left.\frac{\partial x}{\partial m_z}\right|_{m_z=m_z^*} = 0. \quad (\text{B3})$$

Requiring that both entropies at $m_z = 0$ and $m_z = m_z^*$ are equal is analog to solving

$$x|_{m_z=0} = x|_{m_z=m_z^*} \quad (\text{B4})$$

Eq. (B3) and Eq. (B4) are exactly Eq. (46) and Eq. (25).

-
- [1] M. D. Lukin, “Colloquium: Trapping and manipulating photon states in atomic ensembles,” *Rev. Mod. Phys.* **75**, 457–472 (2003).
- [2] M. Saffman, T. G. Walker, and K. Mølmer, “Quantum information with Rydberg atoms,” *Rev. Mod. Phys.* **82**, 2313–2363 (2010).
- [3] Joseph W Britton, Brian C Sawyer, Adam C Keith, C C Joseph Wang, James K Freericks, Hermann Uys, Michael J Biercuk, and John J Bollinger, “Engineered two-dimensional Ising interactions in a trapped-ion quantum simulator with hundreds of spins,” *Nature* **484**, 489–492 (2012).
- [4] Immanuel Bloch, Jean Dalibard, and Wilhelm Zwerger, “Many-body physics with ultracold gases,” *Reviews of Modern Physics* **80**, 885–964 (2008).
- [5] R Blatt and C F Roos, “Quantum simulations with trapped ions,” *Nat. Phys.* **8**, 277–284 (2012).
- [6] C. Monroe, W. C. Campbell, L.-M. Duan, Z.-X. Gong, A. V. Gorshkov, P. W. Hess, R. Islam, K. Kim, N. M. Linke, G. Pagano, P. Richerme, C. Senko, and N. Y. Yao, “Programmable quantum simulations of spin systems with trapped ions,” *Rev. Mod. Phys.* **93**, 025001 (2021).
- [7] Farokh Mivehvar, Francesco Piazza, Tobias Donner, and Helmut Ritsch, “Cavity qed with quantum gases: new paradigms in many-body physics,” *Advances in Physics* **70**, 1–153 (2021).
- [8] Nicolò Defenu, Tobias Donner, Tommaso Macrì, Guido Pagano, Stefano Ruffo, and Andrea Trombettoni, “Long-range interacting quantum systems,” *Rev. Mod. Phys.* **95**, 035002 (2023).
- [9] J Sak, “Recursion Relations and Fixed Points for Ferromagnets with Long-Range Interactions,” *Phys. Rev. B* **8**, 281–285 (1973).
- [10] Michael E. Fisher, Shang-keng Ma, and B. G. Nickel, “Critical exponents for long-range interactions,” *Phys. Rev. Lett.* **29**, 917–920 (1972).
- [11] Erik Luijten and Henk W. J. Blöte, “Classical critical behavior of spin models with long-range interactions,” *Phys. Rev. B* **56**, 8945–8958 (1997).
- [12] Maria Chiara Angelini, Giorgio Parisi, and Federico Ricci-Tersenghi, “Relations between short-range and long-range ising models,” *Phys. Rev. E* **89**, 062120 (2014).
- [13] Nicolo Defenu, Andrea Trombettoni, and Alessandro Codello, “Fixed-point structure and effective fractional dimensionality for $O(N)$ models with long-range interactions,” *Phys. Rev. E* **92**, 289 (2015).
- [14] Nicolò Defenu, Andrea Trombettoni, and Stefano Ruffo, “Anisotropic long-range spin systems,” *Phys. Rev. B* **94**, 224411 (2016).
- [15] Nicolo Defenu, Andrea Trombettoni, and Stefano Ruffo, “Criticality and phase diagram of quantum long-range $O(N)$ models,” *Phys. Rev. B* **96**, 1 (2017).
- [16] Nicolò Defenu, Alessandro Codello, Stefano Ruffo, and Andrea Trombettoni, “Criticality of spin systems with weak long-range interactions,” *Journal of Physics A Mathematical General* **53**, 143001 (2020).
- [17] Thierry Dauxois, Vito Latora, Andrea Rapisarda, Stefano Ruffo, and Alessandro Torcini, *Dynamics and Thermodynamics of Systems with Long-Range Interactions*, edited by Thierry Dauxois, Stefano Ruffo, Ennio Arimondo, and Martin Wilkens (Springer Berlin Heidelberg, Berlin, Heidelberg, 2002) pp. 458–487.
- [18] Alessandro Campa, Thierry Dauxois, and Stefano Ruffo, “Statistical mechanics and dynamics of solvable models with long-range interactions,” *Phys. Rep.* **480**, 57–159 (2009).
- [19] A Campa, Thierry Dauxois, D Fanelli, and S Ruffo, *Physics of Long-Range Interacting Systems* (Oxford Univ. Press, 2014).
- [20] Yan Levin, Renato Pakter, Felipe B. Rizzato, Tarcísio N. Teles, and Fernanda P.C. Benetti, “Nonequilibrium statistical mechanics of systems with long-range interactions,” *Physics Reports* **535**, 1–60 (2014).
- [21] Julien Barré, David Mukamel, and Stefano Ruffo, “Inequivalence of ensembles in a system with long-range interactions,” *Phys. Rev. Lett.* **87**, 030601 (2001).
- [22] W. Thirring, “Systems with negative specific heat,” *Zeit. Phys.* **235**, 339–352 (1970).
- [23] Michael Kastner, “Diverging Equilibration Times in Long-Range Quantum Spin Models,” *Phys. Rev. Lett.* **106**, 130601 (2011).
- [24] Stefan Schütz and Giovanna Morigi, “Prethermalization of atoms due to photon-mediated long-range interactions,” *Phys. Rev. Lett.* **113**, 203002 (2014).
- [25] Stefan Schütz, Simon B Jäger, and Giovanna Morigi, “Dissipation-Assisted Prethermalization in Long-Range Interacting Atomic Ensembles,” *Phys. Rev. Lett.* **117**, 083001 (2016).
- [26] D. Mukamel, S. Ruffo, and N. Schreiber, “Breaking of ergodicity and long relaxation times in systems with long-range interactions,” *Phys. Rev. Lett.* **95**, 240604 (2005).
- [27] F. Borgonovi, G. L. Celardo, M. Maianti, and E. Pederzoli, “Broken ergodicity in classically chaotic spin systems,” *Journal of Statistical Physics* **116**, 1435–1447 (2004).
- [28] Michael Kastner, “Nonequivalence of Ensembles for Long-Range Quantum Spin Systems in Optical Lattices,” *Phys. Rev. Lett.* **104**, 240403 (2010).
- [29] Michael Kastner, “Nonequivalence of ensembles in the curie–weiss anisotropic quantum heisenberg model,” *J. Stat. Phys.* **2010**, P07006 (2010).
- [30] Nicolò Defenu, “Metastability and discrete spectrum of long-range systems,” *Proc. Nat. Acad. Sci.*, In press (2021).
- [31] Alessio Leroose, Tommaso Parolini, Rosario Fazio, Dmitry A. Abanin, and Silvia Pappalardi, “Theory of robust quantum many-body scars in long-range interacting systems,” *Phys. Rev. X* **15**, 011020 (2025).
- [32] Daniel Arrufat-Vicente and Nicolò Defenu, “Freezing and shielding under global quenches for long-range interacting many-body systems,” (2024), arXiv:2407.06072 [quant-ph].
- [33] Nicolò Defenu, David Mukamel, and Stefano Ruffo, “Ensemble inequivalence in long-range quantum systems,” *Phys. Rev. Lett.* **133**, 050403 (2024).
- [34] Victor Bapst and Guilhem Semerjian, “On quantum mean-field models and their quantum annealing,” *J. Stat. Mech.: Theory Exp.* **2012**, P06007 (2012).
- [35] Florent Krzakala, Alberto Rosso, Guilhem Semerjian, and Francesco Zamponi, “Path-integral representation for quantum spin models: Application to the quantum cavity method and monte carlo simulations,” *Phys. Rev. B* **78**, 134428 (2008).
- [36] T. Jörg, F. Krzakala, J. Kurchan, A. C. Maggs, and J. Pujos, “Energy gaps in quantum first-order mean-field-like transitions: The problems that quantum annealing cannot solve,” *Europhysics Letters* **89**, 40004 (2010).
- [37] D. S. Petrov, “Elastic multibody interactions on a lattice,” *Phys. Rev. A* **90**, 021601 (2014).

- [38] A. Goban, R. B. Hutson, G. E. Marti, S. L. Campbell, M. A. Perlin, P. S. Julienne, J. P. D’Incao, A. M. Rey, and J. Ye, “Emergence of multi-body interactions in a fermionic lattice clock,” *Nature (London)* **563**, 369–373 (2018).
- [39] Wilhelm Zwerger, “Quantum-unbinding near a zero temperature liquid–gas transition,” *Journal of Statistical Mechanics: Theory and Experiment* **2019**, 103104 (2019).
- [40] Axel Griesmaier, Jörg Werner, Sven Hensler, Jürgen Stuhler, and Tilman Pfau, “Bose-einstein condensation of chromium,” *Phys. Rev. Lett.* **94**, 160401 (2005).
- [41] A. Micheli, G. K. Brennen, and P. Zoller, “A toolbox for lattice-spin models with polar molecules,” *Nat. Phys.* **2**, 341–347 (2006).
- [42] K.-K. Ni, S. Ospelkaus, M. H. G. de Miranda, A. Pe’er, B. Neyenhuis, J. J. Zirbel, S. Kotochigova, P. S. Julienne, D. S. Jin, and J. Ye, “A high phase-space-density gas of polar molecules,” *Science* **322**, 231–235 (2008).
- [43] S. Morrison and A. S. Parkins, “Dynamical quantum phase transitions in the dissipative Lipkin-Meshkov-Glick model with proposed realization in optical cavity QED,” *Phys. Rev. Lett.* **100**, 040403 (2008).
- [44] J. Larson, “Circuit qed scheme for the realization of the lipkin-meshkov-glick model,” *EPL (Europhysics Letters)* **90**, 54001 (2010).
- [45] Zemao Wu, Jijie Fan, Xue Zhang, Jiansheng Qi, and Haibin Wu, “Signatures of prethermalization in a quenched cavity-mediated long-range interacting fermi gas,” *Phys. Rev. Lett.* **131**, 243401 (2023).
- [46] Tameem Albash and Daniel A. Lidar, “Adiabatic quantum computation,” *Rev. Mod. Phys.* **90**, 015002 (2018).
- [47] H J Lipkin, N Meshkov, and A J Glick, “Validity of many-body approximation methods for a solvable model,” *Nuclear Physics* **62**, 188–198 (1965).
- [48] N. Meshkov, A. J. Glick, and H. J. Lipkin, “Validity of many-body approximation methods for a solvable model. (II). Linearization procedures,” *Nuclear Physics* **62**, 199–210 (1965).
- [49] A. J. Glick, H. J. Lipkin, and N. Meshkov, “Validity of many-body approximation methods for a solvable model. (III). Diagram summations,” *Nuclear Physics* **62**, 211–224 (1965).
- [50] R. H. Dicke, “Coherence in spontaneous radiation processes,” *Phys. Rev.* **93**, 99–110 (1954).
- [51] Kristian Baumann, Christine Guerlin, Ferdinand Brennecke, and Tilman Esslinger, “Dicke quantum phase transition with a superfluid gas in an optical cavity,” *Nature* **464**, 1301–1306 (2010).
- [52] Renate Landig, Ferdinand Brennecke, Rafael Mottl, Tobias Donner, and Tilman Esslinger, “Measuring the dynamic structure factor of a quantum gas undergoing a structural phase transition,” *Nat. Comm.* **6**, 7046 (2015).
- [53] J Reslen, L Quiroga, and N. F Johnson, “Direct equivalence between quantum phase transition phenomena in radiation-matter and magnetic systems: Scaling of entanglement,” *EPL* **69**, 8–14 (2005).
- [54] Stefan Schütz, Simon B Jäger, and Giovanna Morigi, “Thermodynamics and dynamics of atomic self-organization in an optical cavity,” *Phys. Rev. A* **92**, 063808 (2015).
- [55] Ian D. Leroux, Monika H. Schleier-Smith, and Vladan Vuletić, “Implementation of cavity squeezing of a collective atomic spin,” *Phys. Rev. Lett.* **104**, 073602 (2010).
- [56] Gregory Bentsen, Ionut-Dragos Potirniche, Vir B. Bulchandani, Thomas Scaffidi, Xiangyu Cao, Xiao-Liang Qi, Monika Schleier-Smith, and Ehud Altman, “Integrable and chaotic dynamics of spins coupled to an optical cavity,” *Phys. Rev. X* **9**, 041011 (2019).
- [57] Emily J. Davis, Gregory Bentsen, Lukas Homeier, Tracy Li, and Monika H. Schleier-Smith, “Photon-mediated spin-exchange dynamics of spin-1 atoms,” *Phys. Rev. Lett.* **122**, 010405 (2019).
- [58] Emily J. Davis, Avikar Periwal, Eric S. Cooper, Gregory Bentsen, Simon J. Evered, Katherine Van Kirk, and Monika H. Schleier-Smith, “Protecting spin coherence in a tunable heisenberg model,” *Phys. Rev. Lett.* **125**, 060402 (2020).
- [59] A. Gallemí, G. Queralto, M. Guilleumas, R. Mayol, and A. Sanpera, “Quantum spin models with mesoscopic bose-einstein condensates,” *Phys. Rev. A* **94**, 063626 (2016).
- [60] Tin-Lun Ho, “Spinor bose condensates in optical traps,” *Phys. Rev. Lett.* **81**, 742–745 (1998).
- [61] J. Stenger, S. Inouye, D. M. Stamper-Kurn, H. J. Miesner, A. P. Chikkatur, and W. Ketterle, “Spin domains in ground-state Bose-Einstein condensates,” *Nature (London)* **396**, 345–348 (1998).
- [62] M.-S. Chang, C. D. Hamley, M. D. Barrett, J. A. Sauer, K. M. Fortier, W. Zhang, L. You, and M. S. Chapman, “Observation of spinor dynamics in optically trapped ^{87}Rb bose-einstein condensates,” *Phys. Rev. Lett.* **92**, 140403 (2004).
- [63] H. Schmaljohann, M. Erhard, J. Kronjäger, M. Kottke, S. van Staa, L. Cacciapuoti, J. J. Arlt, K. Bongs, and K. Sengstock, “Dynamics of $f = 2$ spinor bose-einstein condensates,” *Phys. Rev. Lett.* **92**, 040402 (2004).
- [64] T. M. Hoang, M. Anquez, B. A. Robbins, X. Y. Yang, B. J. Land, C. D. Hamley, and M. S. Chapman, “Parametric excitation and squeezing in a many-body spinor condensate,” *Nature Communications* **7**, 11233 (2016).
- [65] Hendrik Weimer, Markus Müller, Igor Lesanovsky, Peter Zoller, and Hans Peter Büchler, “A rydberg quantum simulator,” *Nature Physics* **6**, 382–388 (2010).
- [66] N. Henkel, R. Nath, and T. Pohl, “Three-dimensional roton excitations and supersolid formation in rydberg-excited bose-einstein condensates,” *Phys. Rev. Lett.* **104**, 195302 (2010).
- [67] L. I. R. Gil, R. Mukherjee, E. M. Bridge, M. P. A. Jones, and T. Pohl, “Spin squeezing in a rydberg lattice clock,” *Phys. Rev. Lett.* **112**, 103601 (2014).
- [68] Johannes Zeiher, Peter Schauf, Sebastian Hild, Tommaso Macrì, Immanuel Bloch, and Christian Gross, “Microscopic characterization of scalable coherent rydberg superatoms,” *Phys. Rev. X* **5**, 031015 (2015).
- [69] Y. Y. Jau, A. M. Hankin, T. Keating, I. H. Deutsch, and G. W. Biedermann, “Entangling atomic spins with a rydberg-dressed spin-flip blockade,” *Nature Physics* **12**, 71–74 (2016).
- [70] Sebastian Will, Thorsten Best, Ulrich Schneider, Lucia Hackermüller, Dirk-Sören Lühmann, and Immanuel Bloch, “Time-resolved observation of coherent multi-body interactions in quantum phase revivals,” *Nature* **465**, 197–201 (2010).
- [71] H. P. Büchler, A. Micheli, and P. Zoller, “Three-body interactions with cold polar molecules,” *Nat. Phys.* **3**, 726–731 (2007).
- [72] Lorenzo Del Re, Michele Fabrizio, and Erio Tosatti, “Nonequilibrium and nonhomogeneous phenomena around a first-order quantum phase transition,” *Phys. Rev. B* **93**, 125131 (2016).
- [73] S. Morrison and A. S. Parkins, “Collective spin systems in dispersive optical cavity qed: Quantum phase transitions and entanglement,” *Phys. Rev. A* **77**, 043810 (2008).
- [74] Jayson G. Cosme, Jim Skulte, and Ludwиг Mathey, “Bridging closed and dissipative discrete time crystals in spin systems with infinite-range interactions,” *Phys. Rev. B* **108**, 024302 (2023).

- [75] Fabian Finger, Rodrigo Rosa-Medina, Nicola Reiter, Panagiotis Christodoulou, Tobias Donner, and Tilman Esslinger, “Spin- and momentum-correlated atom pairs mediated by photon exchange and seeded by vacuum fluctuations,” arXiv **2303.11326** (2023).
- [76] Elliott H. Lieb, “The classical limit of quantum spin systems,” *Commun. Math. Phys* **31**, 327–340 (1973).